

GALAXY PHOTOMETRY M. USATOV¹

1. AIMS

The aims of this project are as following:

1. Reduce multi-band (BVR) CCD data of the M 51, M 63, M 106 (NGC 4258) and NGC 4725 galaxies obtained via 0.8-m (30-inch) telescope at the McDonald Observatory (MDO) in Austin, TX.
2. Prepare scientific and color-combined frames.
3. Discuss differences and similarities of galactic features appearing in the images that depend on the wavelength and the galaxy type.
4. Conduct preliminary surface photometry of galaxies.

2. INTRODUCTION

The study of the structure of galaxies enables to test our understanding of the processes responsible for their formation and evolution. Photometry data is capable of revealing important galactic characteristics, such as the mass to light ratio, distribution of its stellar populations, gas and dust. As many of the galactic parameters are correlated, photometric data enables to constrain our models by using scaling laws, such as the fundamental plane of elliptical galaxies, thus, revealing hidden properties and information about their formation and chemical and structural evolution. Perhaps, the most well-known example is the Faber–Jackson relation between the luminosity and the stellar velocity dispersion, $L \propto \sigma^\gamma$ (Faber & Jackson 1976). This relation can be interpreted as a projection of a fundamental plane of elliptical galaxies—a scaling law between non-isophotal radius R , mean surface brightness² μ , and velocity dispersion: $R \propto \sigma^\gamma \mu^\delta$ (Djorgovski & Davis 1987). The introduction of the additional parameter explained any scatter in the original Faber–Jackson relation with high accuracy (Taranu et al. 2015). Metallicity and stellar population distribution also participate in the fundamental plane of ellipticals, implying that their chemical and star formation history is connected to dynamics (de Carvalho & Djorgovski 1989). The study of velocity distribution data constrained via photometry can also provide insights to the properties of supermassive black holes in galactic cores, e.g. Kormendy et al. (1997).

In the process of surface photometry, i.e. photometry of extended objects, the two-dimensional distribution of light is reduced to a one-dimensional matrix of intensities. For most of the galaxy types, due to the Keplerian nature of the orbiting matter, it is possible to fit approximate elliptical isophotes which serve as integration boundaries, as the light distribution is measured in the direction away from the core (Milvang-Jensen & Jørgensen 1999; Schombert & Smith 2012). The main steps of conducting the surface photometry of galaxies are standard CCD reduction routines (flat, dark and bias calibration), co-aligning and combining, sky background subtraction, photometric calibration and presentation, along with interpretation and modeling. This project is focused on the CCD reduction routines of the MDO data and the discussion of galactic features that are dependent on wavelength and galaxy morphology, although preliminary non-calibrated surface photometry will be conducted using instrumental magnitudes.

¹ maxim.usatov@bcsatellite.net

² Apparent magnitude of light detected in the area of a square arcsecond.



FIG. 1.— The 0.76-m telescope in the McDonald Observatory of the University of Austin, TX, USA. The 20 ft dome made by Ash-Domes is shown on the right. Photographs from Winans (2011).

3. EQUIPMENT

This project uses raw data provided by Swinburne Astronomy Online, acquired via 0.76-m (30-inch) telescope at the MDO. The telescope was constructed in the 1970 by Boller and Chivens of South Pasadena, CA, a division of the Perkin-Elmer Corporation. Its main fused silica (quartz) mirror was made from the material remaining from the production, i.e. central hole in the primary mirror, of the much bigger 2.7-m telescope at the MDO. The 0.76-m telescope is located inside the 20 ft dome—see figure 1.

The telescope is equipped with a prime focus corrector (PFC) based $f/3.0$ CCD imaging system in place of the standard Cassegrain secondary. It was built by Philip MacQueen and Charles Claver. The system was optimized for wide-field imaging tasks, and it was originally designed to conduct multi-color survey in the search of cool degenerate stars in the U, B, V, I, MgH ($\sim 5200 \text{ \AA}$) and CaH ($\sim 6830 \text{ \AA}$) bands (Baliber & Cochran 2003). The optical performance is nearly diffraction-limited over a 1.1° field. The front-side illuminated CCD, dubbed LF1 by Claver, is made by Loral Fairchild, with 2048×2048 thick detector array and $15 \mu\text{m}$ square pixels, producing a $46.2' \times 46.2'$ field of view (Claver 1992). It has a read-out noise of $5.87 e^-$ and gain of $1.60 e^- \text{ ADU}^{-1}$, covering wavelengths from 3000 to 10000 \AA ($1 \mu\text{m}$, near-infrared) range (Chonis et al. 2011). The detector is coated with Lumigen to boost quantum efficiency in the ultraviolet range to $\approx 20\%$. The LF1 is a high-quality CCD, with only few bad columns, and some charge traps. The pixel scale measured using the WCS solver script in the Pleiades Astrophoto PixInsight software on one of the FITS files resulted in $1.35 \text{ arcsec px}^{-1}$, which corresponds to the system's effective focal length of 2285 mm. The PFC system is equipped with standard UBVRI Bessel filter set.

4. TECHNIQUE

The tasks of CCD reduction, frame aligning and combining and preliminary surface photometry are done in the Image Reduction and Analysis Facility (IRAF) software (Tody 1993). The IRAF installation used in this project is part of the Ureka distribution, which is a collaboration project of Space Telescope Science Institute (STScI) and Gemini Observatory. Non-scientific presentation frames are color-combined and prepared in PixInsight. For galaxy surface photometry, the IRAF STSDAS (Space Telescope Science Data Analysis System) package is used. SAOImage DS9 and Pixinsight are used for viewing and analyzing FITS images and headers. DS9 outputs correct pixel coordinates that are compatible with IRAF, e.g. for bad pixel map construction.

4.1. LF1 CCD Defects

The data made available from LF1 exhibits an unusual property in the sense that bad columns appear in the flat frames, however not in the object or zero frames. Perhaps, this is due to different exposure dates. Since dark frames aren't available (overscan strip is used) and zero frames do not contain all the 2D structure, bad columns aren't corrected and introduce defects into calibrated images. To correct this, a map of bad pixels, *lf1badpixels.pix*, is constructed manually, with the following columns specified via *a-b* pixel ranges obtained via DS9, as per the IRAF format: x_a , x_b , y_a , y_b :

```
1 2 1 3
52 52 128 2047
53 53 128 193
298 299 1080 2047
684 685 1247 2047
819 820 179 2047
834 835 1682 2047
1106 1107 0 2047
1224 1225 1427 2047
1290 1291 1072 2047
1450 1451 27 2047
1882 1882 728 2047
1883 1883 730 742
```

Data within the bad pixel ranges will be extrapolated by IRAF from neighbor pixels. This appears to correct most issues.

4.2. Zero frames

The IRAF task ZEROCOMBINE is used to combine zero (bias) frames. The following parameters are used (irrelevant parameters are omitted):

```
PACKAGE = ccdred
        TASK = zerocombine

(combine=          average) Type of combine operation
(reject =          minmax) Type of rejection
(ccdtype=          ) CCD image type to combine
(process=          no) Process images before combining?
(scale =          none) Image scaling
(nlow =            0) minmax: Number of low pixels to reject
(nhigh =           1) minmax: Number of high pixels to reject
(nkeep =           1) Minimum to keep (pos) or maximum to reject (neg)
(blank =           0.) Value if there are no pixels
```

Average combining is used to minimize noise. A total of 5 zero frames is averaged in order to produce the master zero frame.

4.3. Flat frames

The characteristic Z-shaped mark on the surface of LF1 is apparent in the flat-field frames. The IRAF task FLATCOMBINE is used to create the master flat frame. The following relevant parameters are used:

```
PACKAGE = ccdred
```

```
TASK = flatcombine
```

```
(combine=          median) Type of combine operation
(reject =          none) Type of rejection
(ccdtype=          ) CCD image type to combine
(process=          no) Process images before combining?
(scale =           mode) Image scaling
(blank =           1.) Value if there are no pixels
```

Flat frames are processed individually per each filter. A total of 5 flat frames is combined per each filter in order to produce the B, V and R master flat frames.

4.4. Calibration

The IRAF task CCDPROC is used to calibrate raw object frames with master frames prepared above. The FITS header of the raw data contains correct LF1 bias and trim sections already:

```
BIASSEC = '[2057:2072,2:2047]'
TRIMSEC = '[2:2047,2:2047]'
```

The following relevant CCDPROC parameters are used, example provided below for the B channel. Object FITS frames have been renamed to allow for batch calibration of all galaxies in the project.

```
PACKAGE = ccdred
TASK = ccdproc
```

```
images =          B_*.fits List of CCD images to correct
(fixpix =          yes) Fix bad CCD lines and columns?
(oversca=          yes) Apply overscan strip correction?
(trim =           yes) Trim the image?
(zero =           yes) Apply zero level correction?
(darkcor=          no) Apply dark count correction?
(flatcor=          yes) Apply flat field correction?
(illumco=          no) Apply illumination correction?
(fringec=          no) Apply fringe correction?
(readcor=          no) Convert zero level image to readout correction?
(scancor=          no) Convert flat field image to scan correction?

(readaxi=          line) Read out axis (column|line)
(fixfile=          lf1badpixels.pix) File describing the bad lines and columns
(biassec=          [2057:2072,2:2047]) Overscan strip image section
(trimsec=          [2:2047,2:2047]) Trim data section
(zero =           Zero.fits) Zero level calibration image
(dark =           ) Dark count calibration image
(flat =           BFlat.fits) Flat field images
(illum =          ) Illumination correction images
(fringe =         ) Fringe correction images
(minrepl=         1.) Minimum flat field value
(scantyp=          shortscan) Scan type (shortscan|longscan)
(nscan =          1) Number of short scan lines

(interac=          no) Fit overscan interactively?
```

```

(funcio=          legendre) Fitting function
(order  =          1) Number of polynomial terms or spline pieces
(sample =          *) Sample points to fit
(naverag=        1) Number of sample points to combine
(niterat=        1) Number of rejection iterations
(low_rej=        3.) Low sigma rejection factor
(high_re=        3.) High sigma rejection factor
(grow   =          0.) Rejection growing radius
(mode   =          ql)

```

A variety of defects remain in the images after calibration. In the B and R channels, the flat appears to overcorrect the dust “donut” at pixel coordinates 1947, 987. None of the target galaxies appear to lie within that region, so it can be ignored for further processing. Several images exhibit strong sky gradient. Some frames (M 63 in B and NGC 4258 in R) show a diagonal streak, satellite or asteroid path, that does not obstruct the galaxy, thus it can be ignored. NGC 4725 images exhibit strong blooming from bright stars. None of the streaks obstruct the galaxy. A special case are R channel images that, after calibration, show maximum pixel values on order of 10^8 , unlike other channels that all fit into 16-bit range. This has been addressed with the bad pixel map described above.

4.5. Co-aligning and Combining

The IRAF task IMCOADD, which is part of the Gemini IRAF package (GEMINI.GEMTOOLS), is used in order to align and combine individual frames per each filter. The following relevant parameters are used while the rest remained default:

```

PACKAGE = gemtools
TASK    = imcoadd

(fwhm   =          1.) FWHMPSF for daofind, in pixels (ref)
(aligne=          twodx) Method for rough alignment of images (wcs|user|...
(rotate =          yes) Assume rotation > 0.5 deg
(scale  =          yes) Allow significant scale differences

```

The FWHM setting of ≈ 1 px was found using the IMEXAM task radial plotting. The *twodx* alignment method is based on the cross-correlation of the two frame subsections for the initial estimate of the transformations: x - y offsets, frame rotation and scaling factors; it does not rely on the WCS information. Upon execution, IMCOADD finds star-like objects in frames via DAOFIND, uses the coordinates to derive transformations, transforms the image. Then, images are averaged by calling the IMCOMBINE task and a cosmic ray events clean-up is attempted (the *fl_add* flag). Given that there are only two frames per channel, the cosmic ray cleaning was not effective, as σ -clipping techniques require more images to work. In some cases IMCOADD failed to co-align frames correctly, e.g. M 51 R channel. PixInsight was used to align those manually via DynamicAlign procedure and then the resulting images were combined in IRAF using the IMCOMBINE task.

4.6. RGB Color Combining and Post-Processing

R, V and B frames combined in IRAF are co-aligned in PixInsight using the StarAlignment procedure. V channel is used as the alignment reference. Resulting co-aligned frames are combined into RGB color image using the LRGBCombination procedure with unity weights, whereby V channel is used for G. For presentation purposes, non-scientific color images are prepared next per each galaxy. First, remaining background gradients are modeled and extracted via PixInsight AutomaticBackgroundExtractor procedure during which the target image is corrected via subtraction and



FIG. 2.— The resulting RGB frames from the MDO 0.76-m telescope data, from left to right: 1) M 51—a Seyfert 2 galaxy, type SA(s)bc, 2) M 63—a SA(rs)bc type galaxy with LINER-type active galaxy nucleus, and 3) M 106—a Seyfert 2 galaxy, type SAB(s)bc. Morphological types as per Blanc et al. (2013) and Crowther (2013).

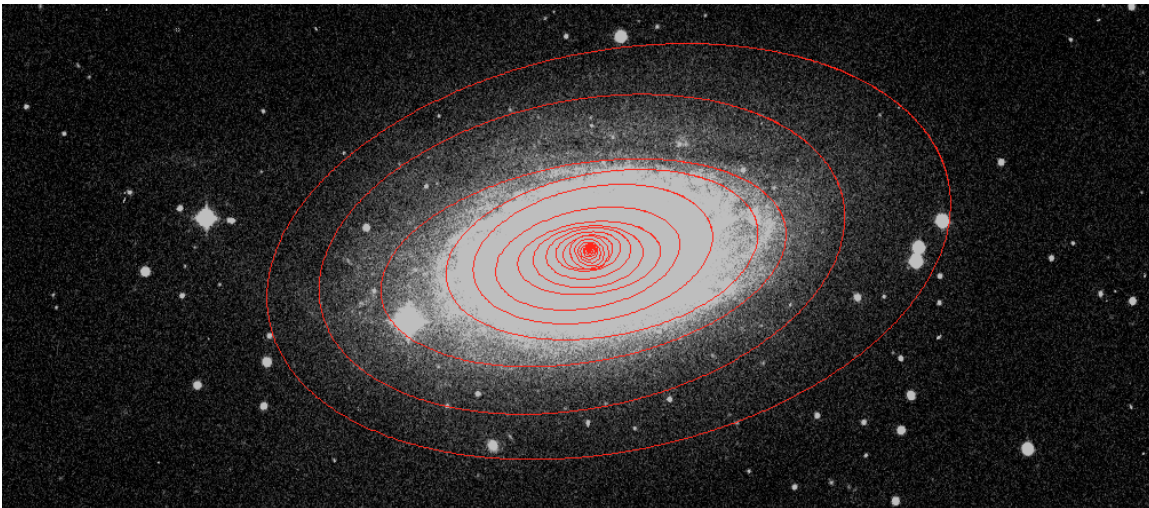


FIG. 3.— Isophote fit to M 63, IRAF task ISOEXAM. Semi-major axis step 0.3. Note this image is a capture from SAOImage DS9 which treats FITS coordinate origin differently to PixInsight that was used to process color-combined images shown in figure 2. This explains the difference in galaxy orientation.

normalized. Rough color calibration is achieved via background color neutralization via Background-Neutralization procedure with the reference image being a preview created from an “empty” patch of the sky of the target image. Upper limit is set to include background sky level. A more sophisticated procedure can be employed to calibrate colors, e.g. $(B - V)$ correction, however rough color calibration is acceptable for non-scientific presentation within the context of this project. Finally, STF settings are used in the HistogramTransformation procedure to stretch histogram into acceptable screen values, with target sky background level of $\approx 10\%$, and the image is saved as JPEG with maximum quality. For the collage of three galaxies in the report (figure 2), Auto Tone correction was applied in Adobe Photoshop.

5. DATA REDUCTION

Co-aligned and combined V-band science frames obtained at § 4.5 is used for preliminary surface photometry run with IRAF STSDAS.ISOPHOTE.ELLIPSE package. A most probable distribution in

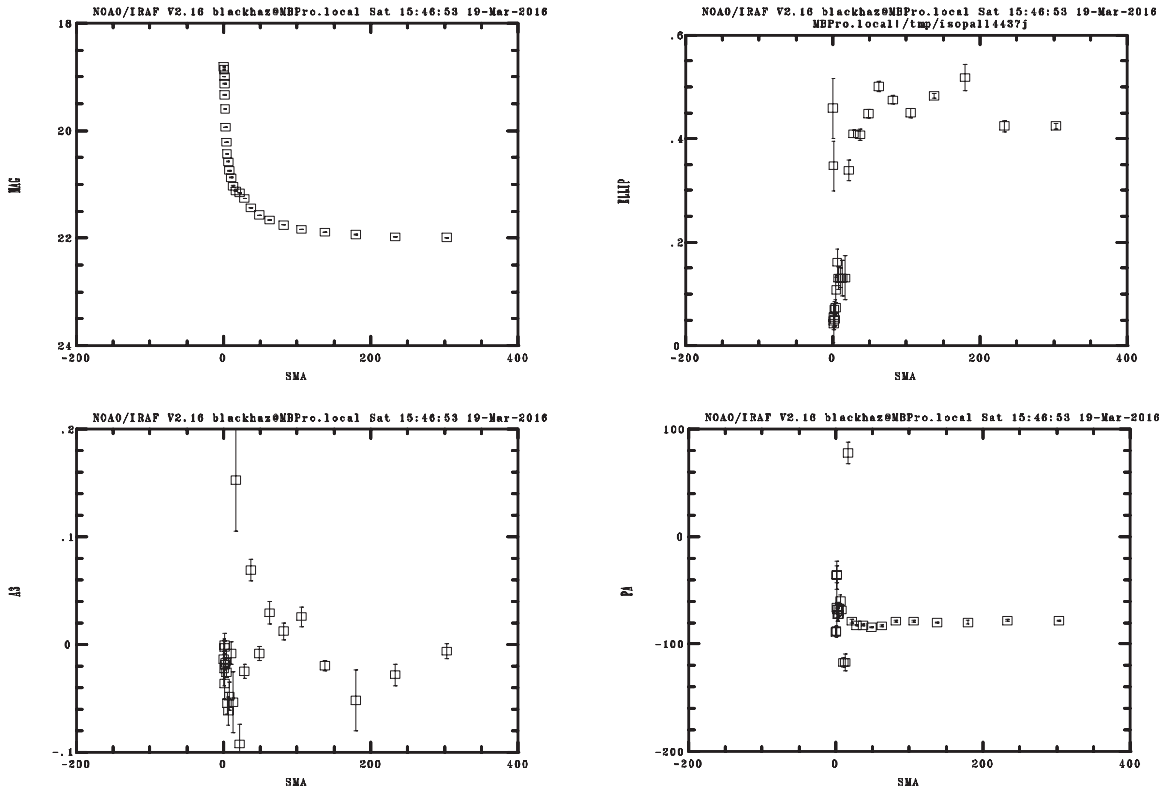


FIG. 4.— Surface photometry for M 63, ISOPALL task output. Description of plots, clockwise starting from the upper left: surface brightness μ (instrumental mag arcsec $^{-2}$), ellipticity, position angle (degrees), and 3rd harmonic deviation from ellipse (A3). Abscissae on all plots are given in semi-major axis, in pixels. Pixel scale is 1.35 arcsec px $^{-1}$.

pixel values (ADUs) is obtained via *mode* measurement of the IMSTAT task. This ADU value is used as the intensity of reference source in MAGPAR to define the magnitude scale. Magnitude of reference source (sky brightness) is assumed to be 22 mag arcsec $^{-2}$. Initial coordinates for the ELLIPSE task are found empirically in DS9. The *step* value in GEOMPAR is set for the isophotes to fit all visible galaxy structure, see figure 3. The results for M 63 are provided in figure 4, which are preliminary and do not represent valid galaxy surface photometry routine. This is because the sky background was not subtracted from the linear frames used, point sources were not removed or masked, defects (mainly cosmic rays) are still present in the frames, and that photometric scale was not calibrated.

6. SOURCES OF ERRORS

The primary sources of errors originate in the signal noise of both random and non-random nature, summarized in the table 1. Random noise sources include the CCD readout noise and the photon noises that follow a Poisson distribution due to random arrival of photons in time. The readout noise depends on the electronic properties of the CCD and is introduced by the on-chip amplifier during the analog-to-digital conversion of signal, as well as the fluctuations of spurious electrons (Howell 2006). The readout noise level was obtained from the FITS header of raw data. A single V-band calibrated frame of M 51 was used to derive the sky background mean value of 4871 ADU. Sky background photon noise, hence, is $\sqrt{4871} = 69.79$ ADU. The mean value within the rectangular region containing galaxy image was found to be 5023 ADU in the same frame, thus, given that ADU counts in the frame represent the sum of the galaxy and the sky background counts (Tonry & Schneider 1988), $5023 - 488 = 152$ (ADU) is the mean contribution of signal from the galaxy, resulting in the object photon noise estimate of $\sqrt{152} = 12.33$ (ADU). Given that the flat-field

TABLE 1
SOURCES OF NOISE

Source	ADU
CCD Readout Noise	3.67
Object Photon Noise	12.33
Flat-Field Photon Noise	N/A
Flat-Field Overcorrection	N/A
Sky Background Photon Noise	69.79
Uncorrected Sky Gradients	N/A
Cosmic Ray Events	N/A
Unmasked Field Objects	N/A

NOTE. — Values are provided in ADU, assuming LF1 CCD gain of $1.60 \text{ e}^- \text{ ADU}^{-1}$. These values are obtained for the single V-Band frame of M 51.

calibration did not achieve perfect removal of dust-caused donuts in the frames, this overcorrection must be an additional source of noise in the frame, along with the strong sky gradients that have not been corrected. Cosmic ray events also contribute noise, given that their removal via σ -clipping was not successful with only two object frames available per channel. Finally, field objects not associated with the target galaxy, such as stars and background galaxies, are another source of errors, as they haven’t been masked in the preliminary photometry run.

7. WAVELENGTH-DEPENDENT FEATURES

The R, V and B bands are capable of revealing wavelength-dependent features in the galactic emission dominated by starlight in the optical range, see figure 5. Given that stars radiate as blackbodies, i.e. their emission can be approximated by Wien’s law $\lambda_{max} = \frac{b}{T}$, the B band frames are dominated by radiation coming from young and hot (blue) stars, such as O and B class stars; while the intensity of the light coming from stars of lower temperatures, e.g. K and M classes, will peak in the R band. Radiation from star-forming regions (SFRs), rich in the H II gas, has a strong wavelength signature in the R filter band because hydrogen, ionized by the UV radiation coming from nearby OB stars, emits strongly at 6563 \AA . A number of other emission features fall within the optical range, summarized in table 2. Interstellar dust is a prominent absorber in optical images of galaxies, appearing as dark streaks superimposed on bright background. As the light attenuation is stronger at shorter wavelengths, dust features appear to be more pronounced in the B band (Mackie 2011).

7.1. M 51

M 51, known as the “Whirlpool,” is a galaxy of type SA(s)bc, hosting a Seyfert 2 nucleus, seen nearly face-on, appearing to be interacting with a smaller companion NGC 5195 (Mackie 2011; Matsushita et al. 2015). All bands reveal the galaxy’s grand-design spiral morphology, with prominent pair of spiral arms, one of which extends to NGC 5195. In grand design galaxies, long-lived perturbations push giant molecular clouds (GMCs) and, hence, SFRs, into their spiral arms (Dobbs et al. 2010). That the spiral arms exhibit a strong, tracing blue component confirms the presence of hot, OB type stars there. Although not prominent on the MDO data, higher-resolution R band images of M 51 reveal the abundance of star-forming H II regions in its spiral arms (Usatov et al. 2010). M 51’s H II regions are also found to be present close to its nucleus (Diaz et al. 1991). Given that the brightness is scattered across the galaxy, it appears that both hot/young and cool/old stars are coupled via density waves, as stellar light distribution in both R and B bands traces the dust lanes and grand-design spiral structure, as suggested by Jarrett et al. (2003).

7.2. M 63

M 63 is a SA(rs)bc type galaxy with LINER-type active galaxy nucleus, known as the “Sunflower galaxy.” It was found to have a warped neutral hydrogen disk extending about twice the radius

TABLE 2
COMMON GALAXY EMISSION FEATURES IN OPTICAL WAVELENGTHS

Source	Wavelength(s), Å
Balmer series H α , H β , H γ	6563, 4861, 4340
He I and He II	5876 and 4686
[O III] ^a	4959, 5007
[N II]	6548, 6583
[O II]	3726, 3729
[S II]	6716, 6731

^aBrackets denote forbidden line, not normally found on Earth. Normally, within conditions found on Earth, atoms would be collisionally de-excited from their metastable states without being able to emit a photon at these wavelengths. In interstellar medium conditions, however, collisions are rare, allowing atoms to decay and emit spontaneously over a long time frame (de Pater & Lissauer 2015).

of the stellar disk (Bosma 1981). Its tightly wound, discontinuous spirals arms and the abundance of irregular, optically thick dust deposits enable M 63 to be classified as a flocculent design galaxy (Elmegreen & Elmegreen 1987). The dust absorption is especially prominent in the B band, along with the surface brightness transition between the inner bright disk at $\sim r/5$, surrounding the nucleus, and the rest of the spiral structure. As the inner disk region is also bright in the V and R bands, it can be concluded that a significant proportion of light and, thus, galactic mass, is concentrated there. The dust absorption is strong below the semi-major axis, thus, that region should be the near side of the galaxy. Although not very prominent on the MDO data, numerous H II regions can be seen in the R band in the spiral arms, tracing sites of on-going star formation.

7.3. M 106

M 106 (NGC 4258) is active LINER-type galaxy, type SAB(s)bc, observed at the inclination angle of $\sim 70^\circ$ (Mackie 2011). The B band image reveals two distinct and thin spiral arms, transitioning into a fainter outer uniform disk that is more pronounced in V and R images. H II emission is evident in R band, tracing SFRs in spiral arms to the galaxy's outermost radii. Dust absorption is prominent in the B band, partially obscuring bright nucleus region. That the dust obscures bright features below the major axis, as seen on the MDO data, allows to conclude that we are looking at the near side of the galaxy in that region, while the far side is above the axis (Jiménez-Vicente et al. 2010).

8. CONCLUSION

The multi-band CCD data from MDO has been reduced and combined into RGB color images for four galaxies. Three of the galaxies—M 51, M 63 and M 106—were analyzed further. Preliminary surface photometry run was conducted for M 63. It was found that more science frames are required in order to successfully remove all the defects, such as cosmic rays, in the images and minimize sources of errors, as σ -clipping techniques are not working with only two frames per channel. Reducing CCD data with only overscan strip information and no dark frames also proves to be more difficult, as manual bad pixel maps have to be constructed to remove bad column defects. IRAF is a great software that allows execution of standardized reduction procedure, however it was found that a GUI-based tool, such as PixInsight, is preferred for RGB-combining and preparation of non-scientific presentation frames, as it allows real-time preview of color manipulation routines, e.g. histogram stretch. As all three galaxies are of spiral type, they exhibit strong similarities in terms of features observed. B band images reveal spiral arms and dust absorption at most, while R band images show H II emission. The strength of absorption enables to determine galaxy orientation in perspective when observing at high inclination angles.

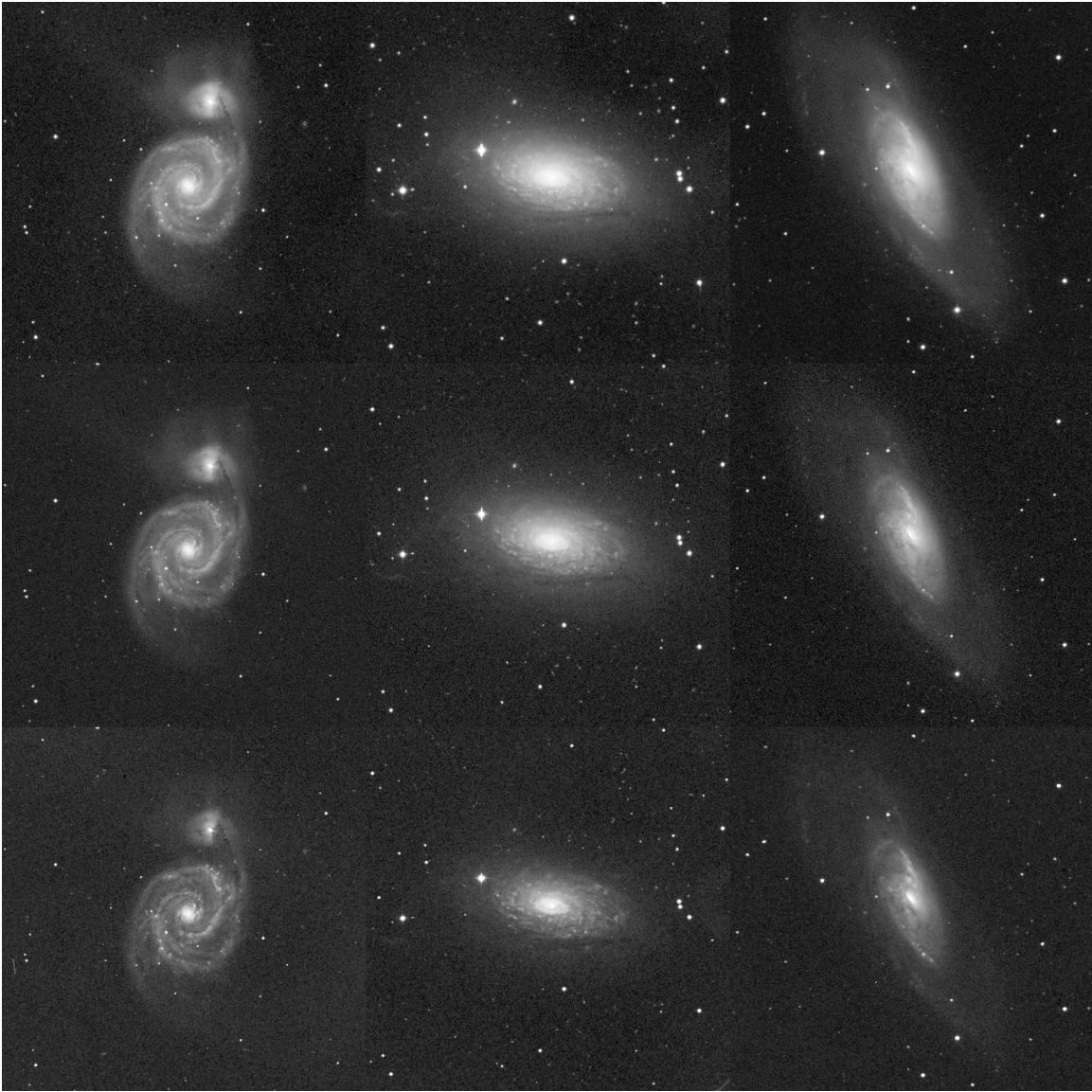


FIG. 5.— Wavelength-dependent features of (left to right) M 51, M 63 and M 106. Top row: R band, middle row: V band, bottom row: B band.

This research has made use of NASA’s Astrophysics Data System Bibliographic Services and the SIMBAD database, operated at CDS, Strasbourg, France. IRAF is distributed by the National Optical Astronomy Observatories (NOAO), which are operated by the Association of Universities for Research in Astronomy, Inc. (AURA), under cooperative agreement with the National Science Foundation. STSDAS is a product of the STScI, which is operated by AURA for NASA.

REFERENCES

- Baliber, N. R., & Cochran, W. D. 2003, in *Astronomical Society of the Pacific Conference Series*, Vol. 294, *Scientific Frontiers in Research on Extrasolar Planets*, ed. D. Deming & S. Seager, 375–378
- Blanc, G. A., Weinzirl, T., Song, M., et al. 2013, *AJ*, 145, 138
- Bosma, A. 1981, *AJ*, 86, 1791
- Chonis, T. S., Martínez-Delgado, D., Gabany, R. J., et al. 2011, *AJ*, 142, 166
- Claver, C. F. 1992, in *Bulletin of the American Astronomical Society*, Vol. 24, *American Astronomical Society Meeting Abstracts*, 1282
- Crowther, P. A. 2013, *MNRAS*, 428, 1927

- de Carvalho, R. R., & Djorgovski, S. 1989, *ApJ*, 341, L37
- de Pater, I., & Lissauer, J. J. 2015, *Planetary Sciences*
- Diaz, A. I., Terlevich, E., Vilchez, J. M., Pagel, B. E. J., & Edmunds, M. G. 1991, *MNRAS*, 253, 245
- Djorgovski, S., & Davis, M. 1987, *ApJ*, 313, 59
- Dobbs, C. L., Theis, C., Pringle, J. E., & Bate, M. R. 2010, *MNRAS*, 403, 625
- Elmegreen, D. M., & Elmegreen, B. G. 1987, *ApJ*, 314, 3
- Faber, S. M., & Jackson, R. E. 1976, *ApJ*, 204, 668
- Howell, S. B. 2006, *Handbook of CCD Astronomy*, ed. R. Ellis, J. Huchra, S. Kahn, G. Rieke, & P. B. Stetson
- Jarrett, T. H., Chester, T., Cutri, R., Schneider, S. E., & Huchra, J. P. 2003, *AJ*, 125, 525
- Jiménez-Vicente, J., Mediavilla, E., Castillo-Morales, A., & Battaner, E. 2010, *MNRAS*, 406, 181
- Kormendy, J., Bender, R., Magorrian, J., et al. 1997, *ApJ*, 482, L139
- Mackie, G. 2011, *The Multiwavelength Atlas of Galaxies*
- Matsushita, S., Trung, D.-V., Boone, F., et al. 2015, *ApJ*, 799, 26
- Milvang-Jensen, B., & Jørgensen, I. 1999, *Baltic Astronomy*, 8, 535
- Schombert, J., & Smith, A. K. 2012, *PASA*, 29, 174
- Taranu, D., Dubinski, J., & Yee, H. K. C. 2015, *ApJ*, 803, 78
- Tody, D. 1993, in *Astronomical Society of the Pacific Conference Series*, Vol. 52, *Astronomical Data Analysis Software and Systems II*, ed. R. J. Hanisch, R. J. V. Brissenden, & J. Barnes, 173
- Tonry, J., & Schneider, D. P. 1988, *AJ*, 96, 807
- Usatov, M., Kuznetsov, A., Satovskyy, B., et al. 2010, *Ultra Deep M51*
- Winans, D. 2011, *30 Inch (0.8 meter) Telescope for University of Texas, McDonald Observatory*